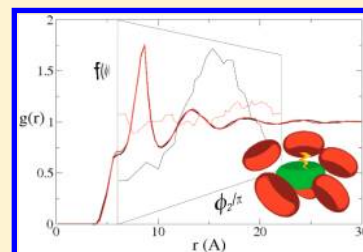


Experimental Evidence of the Relevance of Orientational Correlations in Photoinduced Bimolecular Reactions in Solution

Gonzalo Angulo,^{*,†} Alejandro Cuetos,[‡] Arnulf Rosspeintner,[§] and Eric Vauthey[§][†]Institute of Physical Chemistry, Polish Academy of Sciences, Kasprzaka 44/52, 01-224 Warsaw, Poland[‡]Department of Physical, Chemical and Natural Systems, Universidad Pablo Olavide, 41013 Sevilla, Spain[§]Department of Physical Chemistry, University of Geneva, 30 Quai Ernest-Ansermet, 1211 Geneva 4, Switzerland

S Supporting Information

ABSTRACT: A major problem in the extraction of the reaction probability in bimolecular processes is the disentanglement from the influence of molecular diffusion. One of the strategies to overcome it makes use of reactive solvents in which the reactants do not need to diffuse to encounter each other. However, most of our quantitative understanding of chemical reactions in solution between free partners is based on the assumption that they can be approximated by spheres because rotation averages their mutual orientations. This condition may not be fulfilled when the reaction takes place on time scales faster than that of molecular reorientation. In this work, the fluorescence quenching of two very similar polyaromatic hydrocarbons with different electric dipole moments is measured. The concentration of a liquid electron-donating quencher is varied from very dilute solutions to pure quencher solutions. In both cases, the thermodynamics of the reactions are very similar and, according to the Marcus expression, the kinetics are expected to proceed at similar rates. However, one of them is 10 times faster in the pure quencher solution. This difference starts at relatively low quencher concentrations. An explanation based on the fluorophore–solvent dipole–dipole interaction and the consequent orientational solvent structure is provided. The orientational correlation between fluorophore and quencher is calculated by means of computer simulations. Important differences depending on the fluorophore dipole moment are found. The kinetics can be explained quantitatively with a reaction–diffusion model that incorporates the effects of the presence of the dipole moment and the rotational diffusion, only in the highest quencher concentration case, but not in dilute solutions, most likely due to fundamental limitations of the kinetic theory.



INTRODUCTION

Extracting the intrinsic chemical reactivity from the kinetics of freely diffusing reactants in liquid solution is not a simple task. As the influence of diffusion may mask the reactivity, several strategies have been proposed and applied to circumvent this problem. One of them consists of chemically linking the partners^{1–3} though the influence of the ensuing molecular modifications poses additional interesting questions, like the role in the transfer reaction of the bridge linking the donor and acceptor moieties, or the associated spin dynamics.^{4,5} Another option is to freeze the solution^{6,7} but this changes considerably the properties of the medium. Nowadays it is also possible to explore the time scales on which the molecular translation has not yet started, influencing the reaction using ultrafast spectroscopy. In this latter case, the concentration of the reactant, a fluorescence quencher, has to be increased to observe the so-called “static” reaction regime, in principle free of the influence of diffusion. The ultimate limit is of course a solvent which is reactive itself. Several experimental and theoretical works have explored this approximation, leading to very interesting results and opening more new questions as the dynamics obtained were not as simple as expected. For instance, Yoshihara and co-workers^{8,9} interpreted their data in terms of the two-dimensional Sumi–Marcus model of electron transfer.¹⁰ In the two-dimensional model, there are two

reaction coordinates: one due to the solvent polarization and a second due to the low frequency modes of the reacting system with two corresponding reorganization energies. Fleming’s group proposed a coupling to the solvation dynamics of the fluorophore using nonlinear response functions expressed in terms of both solvation dynamics and reaction kinetics.¹¹ Castner et al. proposed a dynamical electronic coupling matrix element modulated by both inner-sphere and outer-sphere nuclear dynamics.¹² A similar idea can be found in the works by Tachiya and Scherer who incorporated several dynamic variables to the problem, giving special relevance to the different contributions to the reorganization energy from intramolecular vibrations, relative motion of donor and acceptor and the rearrangement of the solvent.^{13,14} Kuzmin and co-workers considered a continuous distribution of matrix coupling elements due to the statistical distribution of reacting pairs.¹⁵ Finally, Vauthey et al. proposed a simple model with different solvation layers to explain the difference observed in the quenching dynamics of perylene (PER) and 3-cyanoperylene (CNPER) in anilines.^{16,17} This latter example has the advantage of keeping most of the parameters of the reaction constant on changing the system, the dipole moment of the

Received: March 13, 2013

Published: August 8, 2013



fluorophore and therefore the solvation around it being the major difference. The question posed is whether the differences in the cybotactic region come from a higher quencher density around CNPER or from an orientational correlation that favors the reaction. If so, and as the reaction takes place on the time scale of molecular rotation, this factor should also be taken into account.

Even though nowadays the position of atoms in molecules can be assessed by crystallographic methods and their shape envisaged by atomic force microscopy,¹⁸ the most developed statistical models accounting for bimolecular chemical reactions in solution, with few exceptions,^{19–21} still treat them as spheres and consider the environment as a structureless liquid.^{22,23} This useful simplification is based upon the fact that rotational diffusion averages orientations faster than molecules approach each other by translational motion.²² Moreover, even if this was not the case, the multitude of possible relative orientations between the two reaction partners washes out the effect of any particular orientation. This had already been considered by Smoluchowski in his seminal work²⁴ describing the coagulation of colloid particles, entities much bigger than the solvent molecules and of a well approximated spherical shape. Despite the disparity of sizes between colloids and molecules, the kinetic theory of diffusion influenced reactions expanded using the same assumptions, namely spherical solutes and a continuum solvent. However, the general opinion in the field has been that these assumptions do not greatly hinder the applicability of the models, as reflected in the chapter devoted to them by S. A. Rice in his influential book, in which he considers quite unlikely the rotational effects to be important for reactions involving hydrocarbons in liquid solutions.²² On the other hand, the positional correlations driven by the solvent structure have recently been considered to explain experimental results.^{25,26} The complete mathematical formalism entangling all diffusion modes, translational and rotational, has been well summarized by Zhou and Szabo²⁷ but, to the best of our knowledge, has not been exploited experimentally yet, at least for molecules not much bigger than the solvent. Since then, the theoretical study of diffusion influenced reactions has lived a major revolution and normalization process.²³ The advent of encounter theories has made it possible to introduce almost any reactivity, either distance dependent or spin-state dependent,^{28,29} as well as liquid structure and hydrodynamic effects.^{25,30–32} In fact, the influence of orientation has been treated in this context for rationalizing the enzyme–protein interactions (or, in general, spherical reacting entities with active and nonactive sites)^{21,33–36} and linked reactants systems.^{37,38} However, the question about the simpler molecular systems, classically studied in liquid solutions, remains unanswered.

According to Rice, molecular rotations average on the 100 ps time scale in low viscosity solvents.²² Therefore, their effects should be appreciable on picosecond and subpicosecond time scales. The question is if the effects of preferential orientations in photoinduced chemical reaction kinetics would be recognized or if they would simply pass for a numerical correction factor in the reactivity. In fact, this latter approach has already been suggested and incorporated in the spherical problem.³⁹ To discriminate between these two possibilities, one would need to compare two reacting systems differing only in their rotational diffusivity or in the intermolecular interactions. Additionally, changes in molecular structure usually lead to changes in their dipole moments. In fact, dipole–dipole

interactions greatly affect molecular solvation and rotation, creating orientational correlations in a liquid that configure its structure around the solute. Moreover, it has been theoretically shown how the dipole moment may affect the reactivity, as in the case of electron transfer.⁴⁰

In the case of electron transfer, several works have already pointed out the importance of the relative orientation to the reactivity and consequently to the kinetics. Marcus et al. explicitly derived the expressions for the coupling matrix elements as a function of the angle between the reactants.⁴¹ Fayer and co-workers developed a formalism for the case of randomly distributed anisotropic reactants in frozen solutions.⁴² Additionally, Scherer has recently analyzed the quenching kinetics in *N,N*-dimethylaniline. The electronic states were calculated quantum mechanically as well as the coupling matrix element, whereas the diffusion was treated classically by means of molecular dynamics simulations.¹³

To determine the extent of the influence of the orientational correlations in the liquid phase, we have chosen fluorophores of very similar characteristics, PER and CNPER. Still, the reaction has to be as simple as possible, as is the case of electron transfer or charge shift. Besides, the reaction has to proceed on a very short time scale as compared to translational diffusion; this can be accomplished by using a reacting solvent like *N,N*-dimethylaniline (DMA).^{12,14,16,17,43} In fact, a difference in the solvation of PER and CNPER in DMA has been suggested to explain the almost 10-fold difference in their fluorescence decays.^{16,17} How should this difference be quantified in the context of diffusion? And more importantly, is this difference also present at low quencher concentrations? In other words, are rotational diffusion, mutual orientation, and liquid structure influencing the bimolecular reactions more than suspected? If this is the case, the interpretation of a number of experimental results should be revised to take these issues into account. This work is an attempt to assess the limits of this effect.

The article is organized as follows: we first describe the experimental procedures and the details concerning the Monte Carlo (MC) simulations of the liquid structure. The diffusional model that introduces the mutual orientation of the reactants and the excluded volume effects through the liquid structure and the rotational diffusion is also presented. In the next section, the results of the MC simulations and of the time-resolved experiments in pure DMA, as well as the Stern–Volmer plots obtained by decreasing the DMA concentration, are presented. The consequences of the structures around the two different fluorophores obtained from MC simulations as well as the reactivity model are then explained. This reactivity model is embedded into a reaction–diffusion model. Finally, the experiments are compared to the calculations performed using the former model, and the limitations and advantages of the model are discussed.

■ EXPERIMENTS AND METHODS

Experimental Section. Perylene (PER) was purchased from Aldrich and recrystallized in benzene. 3-Cyanoperylene (CNPER) was synthesized and purified according to ref 44. *N,N*-Dimethylaniline (DMA) was purchased from Aldrich and distilled under reduced pressure. Benzylacetate (BA) was purchased from Aldrich and used as received. The choice of BA as cosolvent is based on its similar macroscopic characteristics to DMA. Moreover, it is also an aromatic solvent, has a similar molecular size and its electric dipole moment is very close to that of DMA (cf. Table 1 and Scheme 1). The major

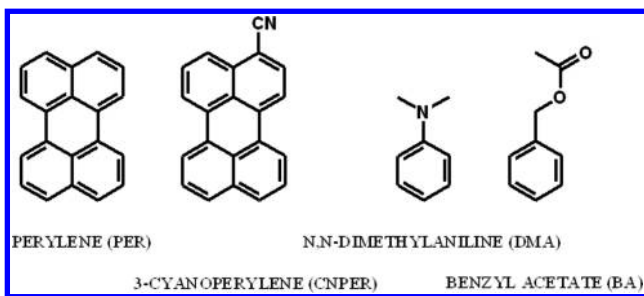
difference between BA and DMA is thence the oxidation potential and therefore their ability as electron donors.

Table 1. Properties of PER, CNPER, DMA, and BA

		Fluorophores					
μ , D	E_{red} , V (vs SCE)	τ , ns	$E(S_1)$, eV	ΔG_{ET} , eV ($\epsilon_S = 37.5$)	ΔG_{ET} , eV ($\epsilon_S = 5$)		
Pe	0	-1.67	4.4	2.8	-0.44	-0.13	
PeCN	4.2	-1.36	4.6	2.6	-0.54	-0.22	
Solvents							
μ , D	E_{red} , V (vs SCE)	n_D^d	ϵ_S^d	τ_L , ps	η , cP ^d	ρ , g/mL ^d	
DMA	1.61	+0.81 ^a	1.558	4.97	15 ^c	1.41	0.956
BA	1.22	+2.56 ^b	1.523	5.1	10.7 ^e	2.32	1.051

^aFrom ref 60. ^bPeak potential from ref 61. ^cFrom ref 62. ^dFrom ref 63. ^eFrom ref 64

Scheme 1. Chemical Structures of PER, CNPER, DMA, and BA



The stationary absorption spectra were recorded with a Cary 50 spectrophotometer. Steady-state fluorescence was measured with a Cary Eclipse spectrofluorometer. Absorption, fluorescence emission, and fluorescence excitation spectra are given in the Supporting Information. The purity of the fluorophores is high enough not to show any parasitic bands in any cases. DMA, the quencher, was distilled under low pressure and did not show any absorption bands other than those corresponding to the compound in accordance with the literature data. BA was used as received and showed no impurities in the absorption spectra. None of the solvents showed any fluorescence emission when excited at the wavelengths used in this work. Time-correlated single photon counting (TCSPC) measurements were performed using a home-mounted apparatus using PicoQuant laser diodes (395 nm LDH-PC-400B), a Becker-Hickel SPC card, and a water-cooled Hamamatsu MCP-PMT. This arrangement leads to an instrument response function of 70 ps full width at half-maximum (fwhm). Shorter fluorescence decays were recorded with a commercial fluorescence up-conversion (FU) apparatus, pumped by frequency doubled 800 nm 100 fs pulses from a Ti:sapphire laser (Spectra-Physics) working at 80 MHz. The instrument response function of this setup was 200 fs (fwhm).^{16,17} Alternatively, a home-built FU apparatus using a KMLabs Ti:sapphire laser with an instrument response function of 70 fs (fwhm) was used.³²

In the high DMA concentration range, the samples were prepared by adding BA to the pure quencher solutions, whereas the inverse procedure was used in the low DMA concentration range. The fluorophore absorbance at the excitation wavelength of the samples was about 1 on 0.1 cm for the FU measurements and around 0.1 for the steady-state and TCSPC experiments. The FU cells were 0.4 mm thick and were continuously rotated

during the measurements. The samples were purged from oxygen by bubbling Ar for 15 min, except in the high concentration range where the oxygen influence is negligible due to the large reaction yield and fast quenching by DMA. The Stern–Volmer (SV) plots were constructed by integrating the FU decay kinetics normalized to 1 at the instrumental zero time in the large DMA concentration range (up to 1 M DMA) or by integrating the fluorescence spectra in the low concentration range. Whenever the fluorescence decay kinetics expanded beyond the time window of the FU, i.e., 2 ns, they were completed with the TCSPC data to provide kinetics decaying to zero for the integration. As observed in the SV plot, the lack of discontinuities points to a correct data handling.

Monte Carlo Simulations. To assess the relevance and magnitude of the influence of the liquid structure, we have carried out computer simulations to study the differences in fluorophore–quencher positional and orientational correlations for the PER and CNPER systems in pure quencher DMA solutions. For this purpose, Monte Carlo (MC) simulations at constant number of particles, volume, and temperature (MC-NVT) have been carried out. A total of 1500 particles of quencher (DMA) and one particle of fluorophore (PER or CNPER) have been placed in a cubic box of $L_x = L_y = L_z = 6.8$ nm size. Periodic boundary conditions have been applied as usual.⁴⁵ All the particles have been considered as hard oblate spherocylinders.⁴⁶ This is a realistic model for disklike molecules where the particles are modeled with oblate spherocylindrical shape with total diameter D and thickness T (Figure 1 in ref 46 and the bottom panel of Figure 1). As the particles studied in this work have different sizes, an extension of the algorithm for the monodisperse case⁴⁶ has been employed. Besides this, CNPER and DMA have an electric dipole moment in the molecular plane. With these considerations, the intermolecular interaction potential is given by

$$u(\vec{X}) = \infty \quad \forall d_M < T_{ij}$$

$$u(\vec{X}) = \frac{\mu_1 \mu_2}{r^3} [\bar{e}_{m1} \bar{e}_{m2} - 3(\bar{e}_{m1} \bar{e}_r)(\bar{e}_{m2} \bar{e}_r)]$$

$$= \frac{\mu_1 \mu_2}{r^3} [\cos \phi_2 \sin \theta_2 - 3 \sin \theta_2 \cos \phi_2 \times (\cos \phi_2 \sin \theta_2 \sin \theta_1 \cos \phi_1 + \sin \phi_2 \sin \phi_1 \sin \theta_2 \sin \theta_1 + \cos \theta_2 \cos \theta_1)] \quad \forall d_M \geq T_{ij} \quad (1)$$

where r is the distance between the centers of mass of the disks, μ_1 and μ_2 are the norms of the dipole moments, $T_{ij} = 0.5(T_i + T_j)$ is the contact distance between two particles, and T_i (T_j) is the thickness of each species. We have considered a diameter of $D = 10.8$ Å for PER and CNPER, whereas that for DMA and BA has been taken as $D = 6.5$ Å. For all the particles, the thickness was set as $T = 4$ Å. The dimensions of the particles were such as to reproduce the van der Waals volume of the molecules as obtained from a semiempirical quantum mechanical optimization of their ground-state geometries using the AM1 method. d_M is the minimum distance between the central disks of the spherocylindrical particles.⁴⁶ The definition of the remaining geometrical parameters can be found in Figure 1. The dipolar term appears only with CNPER and in the interaction between DMA particles for both cases. Induced dipole contributions and other higher order terms have been neglected. The long-range dipole–dipole interaction

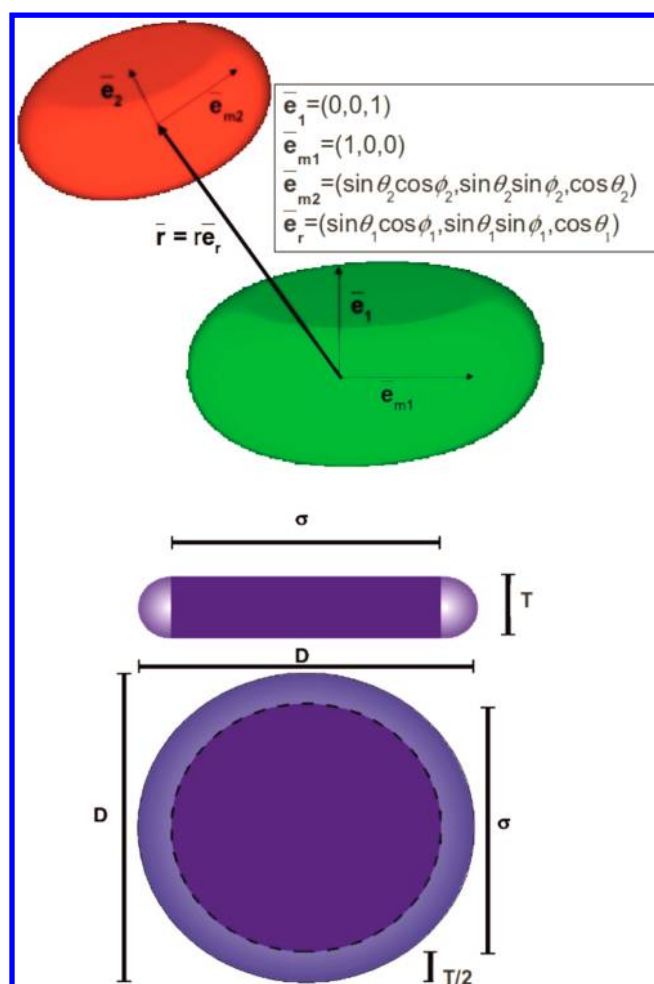


Figure 1. Scheme of the simulated objects and definitions of the geometry (see eqs 1–3 in the text). Top panel: representation of the shape of the particles and the vectors involved in the calculations. The mathematical definition of the vectors is provided in the inset. Bottom panel: Geometrical parameters of oblate spherocylindrical particles. The top and side views of a spherocylinder particle are shown.

was handled with the reaction field method with a dielectric constant of 5 (cf. Table 1).²⁶ The simulations have been done as follows: the position of the unique fluorophore particle was fixed in the center of the simulation box, whereas the DMA molecules could move and rotate freely. 10^6 MC cycles were necessary to thermalize the system, 5×10^6 additional MC cycles were needed to obtain meaningful statistical data. A MC cycle consists of 1500 trials to move and/or rotate a randomly chosen particle. These computer simulations were used in the context of this work to investigate the positional and orientational correlations between fluorophore and quencher molecules. For this, the radial distribution function $g(r)$ and the orientational probability between the dipolar vectors $f(\phi)$ at a given distance have been calculated. Radial distribution functions have been calculated according to

$$g(r) = \frac{1}{4\pi r^2 \rho} \left\langle \sum_j \delta(r - r_{1j}) \right\rangle \quad (2)$$

Here ρ is the density of DMA molecules and r_{1j} is the distance between centers of mass of the fluorophore and of the j th DMA molecule. In the simulation, the Dirac delta function has been replaced by unity in a small range of width $L_x/(2n_{\text{hist}})$ around r ,

with L_x being the size of the simulation box and n_{hist} being the number of divisions used in the histogram set to 100. $g(r)$ was evaluated and accumulated in a histogram with n_{hist} divisions during the simulation. The brackets stand for the ensemble average. $f(\phi)$ was calculated with the expression

$$f(\phi) = \frac{1}{N_j} \langle \delta(\phi - \phi_{1j}) \rangle \quad (3)$$

with the condition that the distance between the particles was in the interval $4 \text{ \AA} < r_{1j} < 6.5 \text{ \AA}$. In this expression $\phi_{1j} = a \arccos(\vec{e}_{m1} \cdot \vec{e}_{mj})$, where \vec{e}_{m1} is a vector in the molecular plane of the fluorophore coincident with the orientation of the dipole for CNPER. \vec{e}_{mj} is the orientation of the dipole in the DMA molecules (Figure 1). N_j is the number of DMA molecules in the simulation box. Again, the Dirac delta has been replaced by unity in a small range of width $2\pi/20$.

Diffusion–Reaction Model. Considering the time window probed in our experiments in pure DMA (up to 50 ps), there is enough time for the molecules to rotate. Furthermore, at lower DMA concentrations, translational motion is also feasible. Therefore, we need to implement these diffusive motions into the model.

As discussed above, the model has to take into account the shape of the molecules with their dipole moments and the interaction due to them between the reactants both in the reactivity and in their motion. We move thus away from the spherical approximation, so the diffusion operator must account for rotational diffusion as well.

In analogy to the differential encounter theory (DET),²² the temporal evolution of the excited fluorophore population (N^*) in a quenching reaction by a species of concentration c is described by

$$\frac{\partial N^*(t)}{\partial t} = -k(t)cN^*(t) - \frac{N^*(t)}{\tau} \quad (4)$$

where τ is the fluorescence lifetime, and $k(t)$ is the time-dependent quenching rate. This quantity is defined as

$$k(t) = \int_{\vec{X}} w(\vec{X}) n(\vec{X}, t) d\vec{X} \quad (5)$$

where $n(\vec{X}, t)$ is the fluorophore–quencher pair distribution function and $w(\vec{X})$ is the intrinsic rate of the elementary reaction responsible for the quenching, charge transfer in the present case. These two quantities depend in principle on all the positional and orientational coordinates of the particles, namely \vec{X} . $n(\vec{X}, t)$ is the solution to the diffusional auxiliary equation

$$\frac{\partial n(\vec{X}, t)}{\partial t} = -w(\vec{X}) n(\vec{X}, t) + \Delta n(\vec{X}, t) \quad (6)$$

To define the diffusional problem, we have considered a fixed reference frame in the fluorophore molecule (Figure 1). The position of the quencher molecule is defined by the position vector of its center of mass, the orientation of the molecule, and the orientation of the dipole. The orientation of the quencher molecule will not be considered explicitly in the solution of the diffusional eq 6. It will be introduced indirectly through steric effects and considered explicitly in the simulations, as explained below. With this, the variables involved in the diffusional problem are $\vec{X} = (r, \phi_1, \theta_1, \phi_2, \theta_2)$. They are the intermolecular distance, the azimuthal and polar angle of the center of mass position vector, and the azimuthal and polar angle of the dipole

of the quencher molecule with respect to the framework defined in Figure 1, respectively (see Figure 1 for more details). The diffusional operator has the form²⁷

$$\begin{aligned} \Delta n(\vec{X}, t) = & D_r \left[\frac{1}{r^2} \frac{\partial}{\partial r} \left(r^2 g(\vec{X}) \frac{\partial n(\vec{X}, t)}{\partial r} \right) \right. \\ & + \frac{1}{r^2 \sin \theta_1} \frac{\partial}{\partial \theta_1} \left(\sin \theta_1 g(\vec{X}) \frac{\partial n(\vec{X}, t)}{\partial \theta_1} \right) \\ & + \left. \frac{1}{r^2 \sin^2 \theta_1} \frac{\partial}{\partial \phi_1} \left(g(\vec{X}) \frac{\partial n(\vec{X}, t)}{\partial \phi_1} \right) \right] \\ & + D_{\theta_2} \frac{1}{\sin \theta_2} \frac{\partial}{\partial \theta_2} \left(\sin \theta_2 g(\vec{X}) \frac{\partial n(\vec{X}, t)}{\partial \theta_2} \right) \\ & + D_{\phi_2} \frac{1}{\sin^2 \theta_2} \frac{\partial}{\partial \phi_2} \left(g(\vec{X}) \frac{\partial n(\vec{X}, t)}{\partial \phi_2} \right) \end{aligned} \quad (7)$$

where $g(\vec{X})$ is the pair distribution function of the liquid that represents its structure. D_r is the mutual translational diffusion coefficient ($65 \text{ \AA}^2 \text{ ns}^{-1}$), and D_{θ_2} (9.1 and 8.0 ns^{-1} for PER-DMA and CNPER-DMA, respectively) and D_{ϕ_2} (18.9 and 11.2 ns^{-1} for PER-DMA and CNPER-DMA, respectively) are the mutual rotational diffusion coefficients.^{16,17} The Supporting Information contains a detailed description of how these parameters have been estimated.

For the solution of the diffusional problem in eq 6, initial and boundary conditions should be specified. The initial condition is explained in the next paragraphs. For the outer boundary condition, a Dirichlet condition has been chosen, i.e., $\lim_{r \rightarrow \infty} n(\vec{X}, t) = 1$. The inner boundary condition for $n(\vec{X}, t)$ is reflective at S , where S is a surface in the variable space separating points not allowed by steric effects from those allowed. This condition ensures that $n(\vec{X}, t) = 0$ in the region not allowed by steric conditions and, at the same time, conserves the particle density. Besides this, periodic boundary conditions have been applied in the angular variables.

For the initial condition of $n(\vec{X}, t)$ ($n(\vec{X}, t=0) = g(\vec{X})$), several approximations have been considered in the past. The simplest is to consider the ideal gas approximation, $g(\vec{X}) = 1$, maybe considering an exclusion area when the particles are very close where $g(\vec{X}_s) = 0$.²² However, it is well-known that the relative radial distribution function of molecules in liquids, at least at short interparticle distances, is not homogeneous.^{25,31,32,47,48} Thus, we have taken the results of the MC simulations to compute it (vide supra). Due to the large number of variables involved, very long simulations would be needed to obtain this quantity with enough statistics in all of them by direct computer simulation. Therefore, an additional approximation has been done using the following expression for $g(\vec{X})$

$$\begin{aligned} g(\vec{X}) = & g(r) F(\vec{X}) K \{1 + \exp[-\beta u(\vec{X})]\} \\ K = & \frac{\int \sin \theta_1 d\theta_1 \sin \theta_2 d\theta_2 d\phi_1 d\phi_2}{\int F(\vec{X}) \{1 + \exp[-\beta u(\vec{X})]\} d\vec{X}} \end{aligned} \quad (8)$$

where $u(\vec{X})$ is the dipolar energy for the configuration \vec{X} , given by eq 1, $\beta = 1/k_B T$, and K a normalization constant. $g(r)$ is the radial distribution function obtained directly by computer simulations (Figure 2). $F(\vec{X})$ is the fraction of configurations

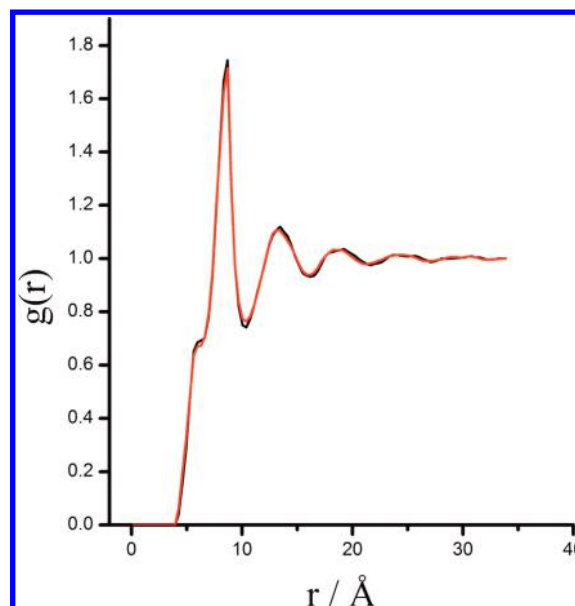


Figure 2. PER-DMA (black) and CNPER-DMA (red) radial distribution functions obtained from MC simulations.

compatible with \vec{X} that are not forbidden by steric effects. To calculate this function, 500 configurations of the quencher molecule compatible with \vec{X} are randomly generated for each set of variables \vec{X} . These configurations are checked for the steric effect allowance using the algorithm described in ref 46. The orientation of the quencher molecule in the diffusional problem is introduced indirectly through $F(\vec{X})$. To check the validity of this approximation, an orientational profile obtained directly by MC simulations is compared in Figure 3 with the one extracted from $g(\vec{X})$ obtained with eq 8. This figure reveals a very good agreement between theory and simulation.

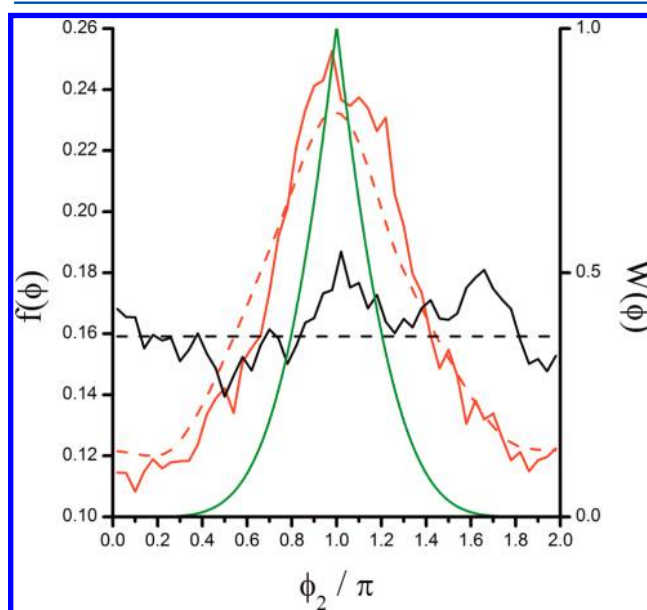


Figure 3. Orientational probability to find the fluorophore (PER, black curve, CNPER, red curve) and DMA dipole vectors at an angle of ϕ . Dashed red line: simulated for CNPER-DMA with eq 8. Dashed black line: $1/2\pi$ dependence for the nondipolar case. The right axes and dark green line correspond to the orientational dependence of the reactivity for CNPER-DMA (eq 10).

For the situation where the concentration of DMA is lower due to the presence of BA, we have used the same function $g(\vec{X})$. This is justified by two reasons: BA and DMA have very similar physical properties (Table 1), and the total density of the system does not change. These facts have as a consequence that the liquid structure around the fluorophore does not change from DMA to BA. In our model, the effect of the decrease in the concentration of DMA is introduced through the explicit dependence on the DMA concentration in eq 4.

Numerical procedures are needed for solving eq 6 with all the conditions explained up to now. For this, the diffusional operator has been discretized on a rectangular grid. For the polar angles, the size of the grid is $\pi/20$ radians, whereas for the azimuthal angles, the size of the grid is $2\pi/20$ radians and, for r , the size of the grid is 0.33 Å. At a maximal distance of 34 Å, the grid was eventually truncated using the Dirichlet boundary condition. With this, the space of variables is discretized in a lattice of $100 \times 20 \times 20 \times 20 \times 20$ points. The time integration was carried out with an Euler algorithm with a time step of 2 fs.

RESULTS AND DISCUSSION

It was already observed in previous works that the fluorescence decay of CNPER in pure DMA is much faster than that of PER^{16,17} (Figure 4). This fact cannot solely be attributed to the

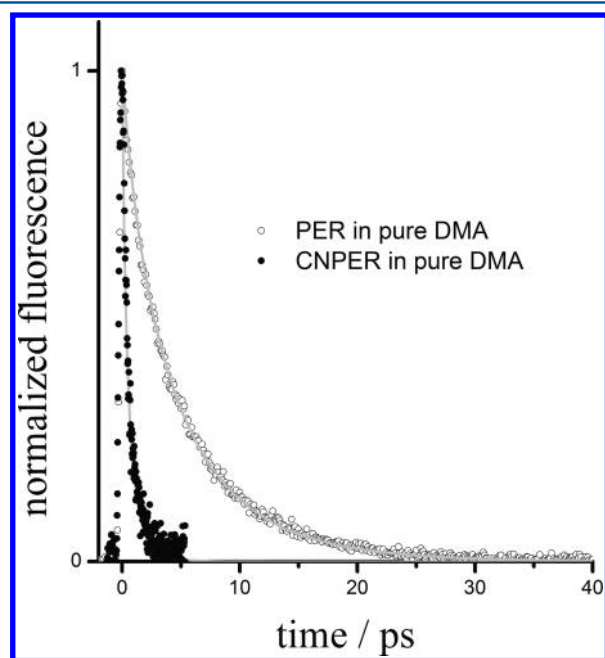


Figure 4. Time profiles of the fluorescence measured at 400 nm excitation of PER and CNPER in DMA. The solid lines are the calculations performed with the model.

difference in driving forces, because, as can be seen in Table 1, they are not sufficiently dissimilar. In fact, the integrated fluorescence intensity of CNPER is almost 1 order of magnitude smaller than that of PER. Both decays are far from being monoexponential and a tentative extraction of a single rate for the reaction has little sense. Another interesting fact is that, on the time scale of these decays, their fluorescence anisotropy has not completely decayed to zero ($\tau_{\text{rot}}/\eta \sim 20\text{--}30$ ps/cP¹⁶), meaning that the reaction is as fast as rotational motion. When the donating solvent is diluted with BA, the difference between the fluorescence decays of both fluoro-

phores decreases but never disappears. At low DMA concentrations, the SV plots (Figure 5, left panel) are much more similar and the rate constants approach the translational diffusion limited rate of $3.3 \times 10^9 \text{ M}^{-1} \text{ s}^{-1}$ (in diffusion limited reactions out of contact as it is the case for charge transfer, rate constants larger than the former value can be observed and depend on the reaction driving force). Because of the similar properties of DMA and BA (Table 1), preferential solvation at lower DMA concentrations, as well as dramatic changes in electron-transfer parameters or in diffusion constants can be excluded as the causes for the observed differences. The fact that the difference in rate constants between PER and CNPER remains over the whole range of DMA concentrations, despite their similar energetics for electron transfer, suggests that this difference must be related to the presence of the dipole moment in CNPER. This dipole moment could introduce two differences in the reactions between PER or CNPER with DMA: (i) the structure of the liquid around the fluorophore and/or (ii) differences in the anisotropy of the reactivity. To check the relative importance of these effects, we have undertaken the theoretical approach described in what follows.

Some of the results of these simulations are shown in Figures 2 and 3. Figure 2 reveals that the fluorophore–DMA radial distribution function is independent of the fluorophore dipole moment. Both reactant systems show a peak at an intermolecular distance of about 8.65 Å. This peak corresponds to an edge-to-edge configuration (both molecules parallel and in contact at the rims). Besides this, a small peak appears at the center-of-mass to center-of-mass distance of 4.5–6 Å. This peak indicates the presence of a small but relevant number of pairs of particles in face-to-face configuration. This configuration is important because, it maximizes the overlap between π -orbitals, and thus their reactivity. The second sphere of coordination is reflected by additional peaks that appear at longer distances. As can be seen in Figure 2, there is no difference between PER (without dipole) and CNPER (with dipole moment). Similar results have been found by computer simulations for the case of pure repulsive spherocylinders.⁴⁶ This indicates that the number of quencher particles at a distance from the fluorophore where the reaction has a high probability is controlled by entropic effects, without a relevant influence of the dipolar interaction. Nevertheless, the relevance of the dipolar interaction emerges when the orientational correlations are explored. The probability to find a fluorophore and DMA molecules with a given angle ϕ between the vectors of their dipoles is shown in Figure 3. In this plot, only pairs of molecules with an intermolecular distance between 4 and 6.5 Å are considered. This interval corresponds to the first peak in the radial distribution function. As mentioned above, at this distance, the molecules are in face-to-face configuration due to steric limitations. If the fluorophore molecule is the nondipolar PER, the orientation probability plotted in Figure 3 is independent of the angle ϕ_2 . In contrast to this, in the case of CNPER, there is a clear orientational correlation between the dipoles of DMA and CNPER in their face-to-face configuration. Furthermore, in this case, the orientational probability shows a clear maximum at $\phi_2 = \pi$ radians. This maximum corresponds to dipoles in antiparallel orientation. As will be shown later, the reactivity is most probably maximized in this configuration.

From the computer simulation results shown so far, it is possible to conclude that the dipole moment of CNPER influences the orientation of the quencher molecules around

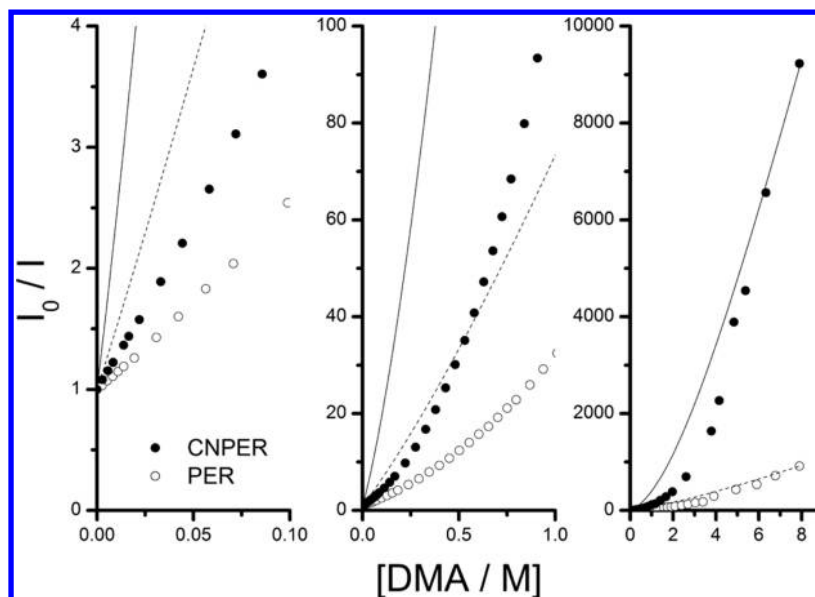


Figure 5. Stern–Volmer plot of the fluorescence quenching of PER and CNPER in DMA-BA mixtures. The lines are the results of the model calculations (dashed for PER and solid for CNPER).

the fluorophore, enhancing the antiparallel dipolar configurations. If this angular configuration has a higher reaction probability than others, the quenching kinetics should be faster. In fact, the preferred orientation, π radians between the dipole moments of the donor and the acceptor, can be thought of as ideal for the electron to be transferred. Indeed, when evaluating the coupling element from the molecular orbitals, one should bear in mind not only the reactants but also the products. As a matter of fact, in electron transfer theory, this quantity stands for the coupling between the free energy surfaces of the reactants with that of the products. In other words, the combined wave functions of the reactants must overlap in space with those of the products to produce a nonzero reaction probability.⁴⁹ The reactivity model presented below, although the simplest possible in our case, assesses the former issues reasonably well. A more detailed and precise one would require careful quantum mechanical calculations, which are beyond the scope of this work.^{12,50–53}

Taking into account that the charge distributions in the neutral and anionic forms of PER are different from those in CNPER, due to the presence of the strong electron-withdrawing nitrile group, we have developed a semiempirical model for the intrinsic rate of charge transfer. A simple semiempirical AM1 calculation is sufficient to see that the electronic density distribution in the educts and products is distributed evenly over the entire PER in both neutral and anionic forms, whereas they are substantially asymmetric for any of the two forms of DMA (larger density near the N in the neutral and in para position with respect to the amino group of the cation) as well as for CNPER, especially in the anionic form (larger density near the CN group). Figure 6 summarizes the reactivity embedded into the diffusional model. For all the molecules studied here, the molecular orbitals involved in the reaction are mostly of π type character and thus the reactivity is expected to be the largest when the molecular planes are parallel. Nevertheless, the reactivity can also be high for an edge-to-edge configuration, as found experimentally.⁵⁴ It should be noted that, because of steric limitations, almost only fluorophore–quencher pairs with face-to-face molecular planes

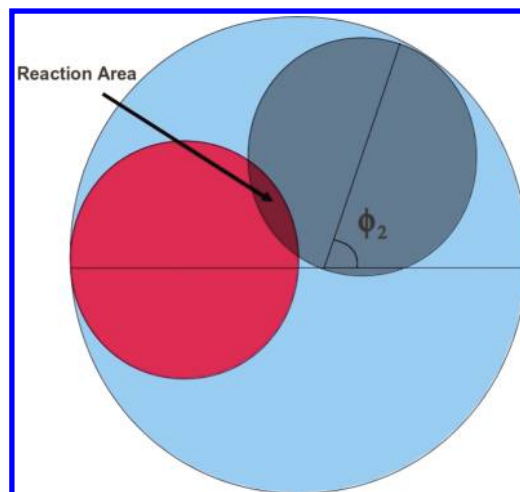


Figure 6. Reactivity model. Red area: reaction zone in the dipolar fluorophore (CNPER). Light blue area: top view of the fluorophore molecule and reaction zone in the nondipolar fluorophore (PER). Dark blue area: top view and reaction zone for quencher molecule. The overlap area for the reaction between CNPER and DMA is pointed out. For the reaction between PER and DMA this area corresponds to the full DMA surface.

(neither tilted nor displaced) are possible when their centers of mass are close. As CNPER and DMA are dipolar, their molecular orbitals are concentrated in one part of the molecular plane, whereas they are distributed over the whole molecular plane for PER. The orbitals are modeled as disks of radius $D_i/2$ for PER and DMA, and of radius $D_i/4$ for CNPER, with D_i being the diameter of each molecule. The reactivity is proportional to the overlap between these orbitals, as schematically shown in Figure 6.

Making use of the above considerations, the following equation for the charge transfer reactivity of PER–DMA is obtained

$$w_{\text{ND}}(X) = w_{0,\text{ND}} e^{-2(r-\sigma)/L} (\sin \theta_2)^2 \quad (9)$$

whereas for CNPER-DMA

$$w_D(X) = w_{0,D} e^{-2(r-\sigma)/L} N (y - \sin y)^2 (\sin \theta_2)^2$$

$$y = 2 \arccos \left[\frac{1}{2} \sqrt{2(1 + \cos \phi_2)} \right]$$

$$N = \frac{2\pi}{11.2462} \quad (10)$$

In both cases, L stands for the decay of the orbital overlap with distance and w_0 is the pre-exponential factor or the reaction frequency multiplied by the Franck–Condon factor. ϕ_2 and θ_2 are defined as above (cf. Figure 1) and N is a normalization factor for the angular integration. Notice the similarity between eqs 9 and 10 and the classical Marcus expression for electron transfer

$$w(r) = \underbrace{\frac{\pi}{k_B T \lambda} e^{-\frac{(\Delta G + \lambda)^2}{4k_B T \lambda}} \frac{V_\sigma^2}{\hbar}}_{w_{0,i}} e^{-\frac{2(r-\sigma)}{L}} \quad (11)$$

Here, i stands for either D (dipolar) or ND (nondipolar), λ denotes the reorganization energy, ΔG is the free enthalpy of reaction, V_σ is the coupling matrix element at contact distance and the other variables and constants have their usual meaning. In essence, our models are mere extensions to the classical expression to account for the angular dependence of the reaction probability within the geometrical discotic model used here. However, we do not explicitly account for any of the variables within $w_{0,i}$. L is strongly affected by the introduction of the angular dependences and therefore cannot be directly compared to the values obtained from purely spherically-symmetrical models (see the Supporting Information for a further discussion about the spherical approximation and how it compares with the present one).

The only values that have to be adjusted to fit the numerical calculations to the experimental results are the electron transfer parameters L and $w_{0,i}$. For the PER-DMA reactivity, the values obtained here are $L = 0.43 \text{ \AA}$ and $w_{0,ND} = 2790 \text{ ns}^{-1}$. For the CNPER-DMA reactivity, $L = 0.86 \text{ \AA}$ and $w_{0,D} = 2000 \text{ ns}^{-1}$. A comparison between the kinetics in pure DMA and the numerical result is depicted in Figure 4. The coincidence is very good. Additionally, these values result in a ratio of the space integrated reactivities given by

$$\int_X w_{ND}(X) dX / \int_X w_D(X) dX = 0.62 \quad (12)$$

This is in very good agreement with the ratio of the factors in the classical Marcus expression (eq 11) considering the difference in driving force (cf. Table 1) and all remaining parameters are equal in both cases. In other words, if both the magnitude and the spatial dependence of the coupling are identical in the spherical approximation (see the Supporting Information), the ratio of the intrinsic electron transfer rates, k_X , is given by

$$k_{PER}/k_{CNPER} = \frac{e^{-(\Delta G_{PER} + \lambda)^2/4k_B T \lambda}}{e^{-(\Delta G_{CNPER} + \lambda)^2/4k_B T \lambda}} = 0.62 \quad (13)$$

taking the values for ΔG listed in Table 1 and λ equal to 0.24 eV, as calculated from the Born approximation. A further comparison of the preexponential factors of eqs 9 and 10 with the classical Marcus expression leads to values of the coupling

matrix element of 11 and 8 meV for PER and CNPER, respectively, which is perfectly within the limits of applicability of the nonadiabatic electron transfer model.⁵⁵ This means that, according to our calculations, both the reorganization energy and coupling matrix element must indeed be very similar, the angular dependence of the reactivity and the orientational correlation between reactants being the only major difference responsible for the huge disparity in kinetics.

The kinetic rate constants amount to $1.1 \times 10^6 \text{ \AA}^3 \text{ ns}^{-1}$ ($0.67 \times 10^{12} \text{ M}^{-1} \text{ s}^{-1}$) and $1.8 \times 10^6 \text{ \AA}^3 \text{ ns}^{-1}$ ($1.08 \times 10^{12} \text{ M}^{-1} \text{ s}^{-1}$) for PER and CNPER, respectively. Both these values and the pre-exponential factors $w_{0,i}$ are of the order of magnitude of the classical nuclear vibrations in aromatic molecules, or frequency factors for the electron transfer reactions, which are claimed to constitute the upper limit for the reaction rate.⁵⁶ If the reaction was limited by the solvent dielectric relaxation time, its rate constant would amount in first approximation to $4.1 \times 10^4 \text{ \AA}^3 \text{ ns}^{-1}$ ($2.5 \times 10^{10} \text{ M}^{-1} \text{ s}^{-1}$). A simplistic analysis of the fluorescence decay profiles of PER and CNPER in DMA gives average decay times of 5.9 and 0.59 ps, respectively, whereas the dielectric relaxation time (τ_L) in DMA amounts to 15 ps. This means that, regardless of the point of view, the reaction is faster than the dielectric relaxation of the solvent and somehow controlled by the internal degrees of freedom. This situation has been observed in many occasions for electron transfer fluorescence quenching and has been given several explanations (vide infra).

The Sumi–Marcus model of multimodal relaxation,¹⁰ used and extended by Barbara and co-workers⁵⁷ as well as by Yoshihara's group^{8,9} for ET in pure donating solvents, has been successfully applied to ET reactions proceeding faster than the solvent relaxation time. In this model, the reaction coordinate is multiple: one due to the solvent reorganization, as in the classical Marcus model, and the others due to internal vibrational modes of low frequency of the reactants. This is most likely also valid in our case. However, this model leads to a time-dependent intrinsic rate constant, the implementation of which, in the already very demanding model proposed by us, would make the calculations numerically unbearable. Most likely, to fully model these kinds of reactions, both factors, orientation correlation and associated rotational motion, and complex time-dependent reactivity, have to be taken into account. However, it should be noted that in these examples, the reactions are faster than in the present case due to larger driving forces. Therefore, in such cases, the role of material diffusion is less important than in the present one and has been omitted.

Another set of factors that has not been considered in the present analysis is related to the internal low frequency modes of the first solvation shell of the reactants and to the associated matrix coupling element. Castner et al.,¹² Tachiya and Scherer^{13,14} and Zinth and co-workers⁵⁸ have stressed the role of intra- and intermolecular vibrations on the temporal modulation of the electronic coupling matrix element. However, again the reactions treated by these groups were found to be significantly faster than those studied here (30–100 fs in refs 58 and 12 compared to 500 fs here). In the present case, cyano-group bending modes (estimated to be at around 150–300 cm^{-1}) might have a significant effect in modulating the instantaneous reaction probability for some mutual orientations of CNPER and DMA. The same might be true for some modes of DMA. To account for these effects, calculation methods that already exist^{50–53} ought to be

considered. However, it is quite likely that, despite being relevant, these effects are time-averaged on time scales shorter than those monitored here. Otherwise, the consistent description of the kinetics provided by our model for PER and CNPER in pure DMA would not be as satisfying as found.

The difference in the reaction yields, as depicted in the Stern–Volmer plots (Figure 5) for PER and CNPER is conserved even down to very low DMA concentrations. It is clear that in the high DMA concentration range, this difference is mostly attributable to the orientational effects that have just been discussed for pure DMA. However, at very low concentrations, this difference should become less and less important. To better compare the steady-state results, we have plotted the ratio of the two concentration-dependent Stern–

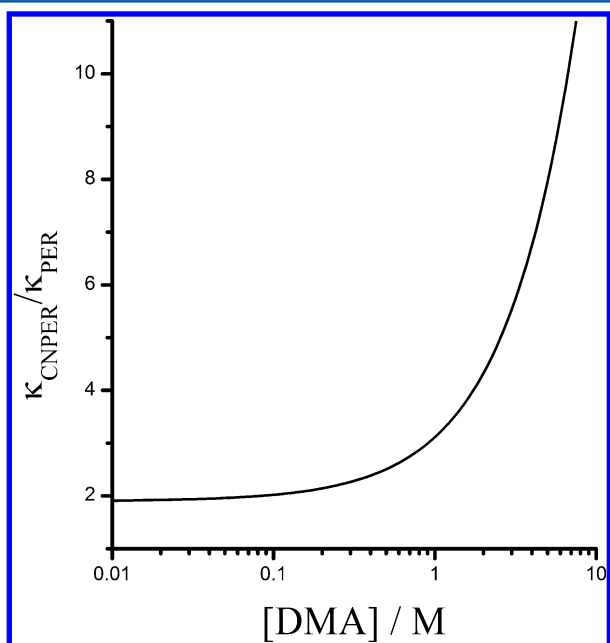


Figure 7. Ratio of the Stern–Volmer constants $\kappa_{\text{CNPER}}(c)/\kappa_{\text{PER}}(c)$ as a function of the quencher concentration. The original experimental data have been interpolated for a clearer comparison.

Volmer constants, $\kappa_X(c)$, in Figure 7, as extracted from the Stern–Volmer equation.

$$\frac{I_0}{I(c)} = 1 + \kappa(c)\tau c \quad (14)$$

where I_0 and $I(c)$ are the steady-state emission intensities in the absence and presence of quencher with concentration c , respectively, and τ is the fluorescence lifetime of the fluorophore. Two interesting facts can be extracted from this figure: First, at low quencher concentrations, the rate constant for CNPER is twice that for PER, this difference remaining constant up to a concentration of approximately 0.1 M. Second, at higher quencher concentrations, the reaction with CNPER becomes up to 10 times faster than that with PER. The difference at low quencher concentrations can be attributed to differences in the intrinsic electron transfer rate constant due to variations in driving force and coupling. Nevertheless, the reaction is still strongly influenced by diffusion and is not purely kinetically controlled, as can be judged from the concentration dependence of the Stern–Volmer constant and the absolute values of the diffusional rate constant, k_{diff} and the Stern–

Volmer rate constant at low concentration, κ_0 . The constant ratio of the rates up to 0.1 M indicates that the spherical approximation suffices in this range to explain the experimental results. However, at higher concentrations, this approximation has to be lifted to rationalize the experimental findings. The reason is that, beyond 0.1 M, the static quenching regime becomes more and more important, revealing the fine details of the early quenching events. In our approach, this is equivalent to having a major contribution from orientational correlations beyond 0.1 M.

We have extended the calculation with our model to cover the entire experimental concentration range. Though the model qualitatively reproduces the trends of both Stern–Volmer plots, the quantitative deviations become larger at lower quencher concentrations. We have tested other parameter values to see if our model could explain the region at low DMA concentrations. It is indeed possible to find pairs of L and w_0 values that better fit the experimental Stern–Volmer plot at low DMA concentrations for both PER and CNPER (see the Supporting Information for further discussion). However, we could not find a complete set of parameters that (i) provides a good agreement between experimental and calculated Stern–Volmer plots at low DMA concentration and (ii) at the same time fulfills the relation of eq 11. Besides this, with all these alternative sets of parameters, the good agreement between experimental and calculated fluorescence decays in the pure DMA solvent is lost.

The fact that the model is able to satisfactorily reproduce the very high concentration range but not the low one, points to three possible explanations. The first is that no hydrodynamic effect on the diffusion translational or rotational coefficients has been introduced. It has been shown that, at low quencher concentrations, this can be quite important and tends to reduce the quenching efficiency.^{25,31,32} The second is related to the way the quencher–quencher excluded volume effect is introduced in the diffusional operator. Despite having been extensively used in the past,^{25,30–32,47} it is known that this approach is not fully theoretically grounded. Currently, attempts to improve the understanding of this effect are under way.⁵⁹ In short, this excluded volume effect, hindering the movement of the particles, is introduced via a potential $g(\vec{X})$ like an electrostatic potential, though it could affect the mathematical form of the diffusion operator in other ways, yet unknown. The third explanation is related to the dynamic nature of the electron transfer variables like the coupling matrix element, V_{σ} . If this quantity or function changes with time as coupled to the molecular dynamics (orientation and internal vibrations of the reactants and solvent molecules), very large coupling elements can be realized on a very short time scale. However, if the molecules have to diffuse from larger distances before encountering each other, the electron transfer occurs before the large V_{σ} configurations can be reached. This would translate into an effective concentration or time-dependent V_{σ} . In other words, large V_{σ} 's would only be accessible at larger concentrations when the relative contribution of the static quenching to the overall quenching process is very important. Additionally to these major issues, it is also possible to consider a different geometrical model for the reactants in which the dipole moments are displaced from the center of the molecules or even slightly out of plane. This would modify the geometry of the reactivity but would not greatly affect the structure of the medium around the dipolar fluorophore.

CONCLUSIONS

We have shown that the fluorescence decays of the nondipolar PER and the dipolar CNPER differ substantially in a pure electron-donating solvent, DMA. They take place on the same time scale as the reorientation dynamics of the reactants. The quencher concentration dependence differs in the entire concentration range, but the difference is constant up to 0.1 M. These findings are intriguing because no large differences are to be expected in view of the energetics of the reaction. A model has been developed that takes into account the liquid structure, with orientational and positional correlations, and their temporal evolution. This implies the necessity to consider the rotational diffusion together with the translational diffusion, the dipole–dipole interaction between reactants and the anisotropic distribution of the reactivity.

The proposed model can explain the kinetics at the highest achievable concentrations of DMA. The model suggests the preorientation of CNPER-DMA pairs to be the reason for the difference in kinetics. Moreover, during the reaction, little translational diffusion (about 1 Å in 50 ps) takes place and not much rotational (about 1 rad in 50 ps for the fastest rotation). At lower concentrations, rotational diffusion starts to lower the efficiency of the reaction and ultimately at very high dilution both reactions take place close to the translational diffusion control regime. The model correctly accounts for the differences in the concentration dependence, although it fails to quantitatively explain the Stern–Volmer plots. Several reasons for this failure have been suggested, the most likely being the limits of the binary theory (diffusional operator) used despite the corrections introduced to account for the steric hindrance of motion and the simplicity of the reactivity model. Further theoretical effort is needed in this respect. More experimental work is desirable though it is difficult to foresee better, or simpler, chemical systems. A further work should be performed using other liquid quenchers or changing the liquid pressure.

ASSOCIATED CONTENT

Supporting Information

Absorption and fluorescence spectra, fluorescence anisotropy decays, estimation of the rotational diffusion coefficients, and comparison of the full roto-translational diffusion model and the spherically symmetrical model. This material is available free of charge via the Internet at <http://pubs.acs.org>.

AUTHOR INFORMATION

Corresponding Author

*G. Angulo: e-mail, gangulo@ichf.edu.pl.

Notes

The authors declare no competing financial interest.

ACKNOWLEDGMENTS

E.V. and A.R. thank the University of Geneva and the Swiss National Science Foundation through the NCCR MUST for financial support. A.C. is thankful for the funding from the Operative Programme FEDER-Andalucia 2007-2013 through project P09-FQM-4938 and from the Spanish Ministry of Science and Innovation (MICINN) through project CTQ2012-32345. The authors thank Dr. Daniel Kattinig for stimulating and helpful discussions.

REFERENCES

- (1) Verhoeven, J. W. From Close Contact to Long-Range Intramolecular Electron Transfer. *Adv. Chem. Phys.* **1999**, *106*, 603–644.
- (2) Closs, G. L.; Calcaterra, L. T.; Green, N. J.; Penfield, K. W.; Miller, J. R. Distance, Stereoelectronic Effects, and the Marcus Inverted Region in Intramolecular Electron Transfer in Organic Radical Anions. *J. Phys. Chem.* **1986**, *90*, 3673–3683.
- (3) Staerk, H.; Kuehnle, W.; Weller, A.; Werner, U. Electron Transfer and Magnetic Field Effects in Donor-Acceptor Systems Linked by a Hydrocarbon Chain Incorporating Phenyl Groups. *Z. Phys. Chem. (Munich)* **1995**, *188*, 61–73.
- (4) Scott, A. M.; Miura, T.; Ricks, A. B.; Dance, Z. E. X.; Giacobbe, E. M.; Colvin, M. T.; Wasielewski, M. R. Spin-Selective Charge Transport Pathways through p-Oligophenylene-Linked Donor-Bridge-Acceptor Molecules. *J. Am. Chem. Soc.* **2009**, *131*, 17655–17666.
- (5) Busmann, H.-G.; Staerk, H.; Weller, A. Solvent Influence on the Magnetic Field Effect of Polymethylene-Linked Photogenerated Radical Ion Pairs. *J. Chem. Phys.* **1989**, *91*, 4098–4105.
- (6) Gray, H. B.; Winkler, J. R. Long-Range Electron Transfer. *Proc. Natl. Acad. Sci. U. S. A.* **2005**, *102*, 3534–3539.
- (7) Gomes, P. J. S.; Serpa, C.; Nunes, R. M. D.; Arnaut, L. G.; Formosinho, S. J. Exothermic Rate Restrictions in Long-Range Photoinduced Charge Separations in Rigid Media. *J. Phys. Chem. A* **2010**, *114*, 2778–2787.
- (8) Yoshihara, K.; Tominaga, K.; Nagasawa, Y. Effects of the Solvent Dynamics and Vibrational Motions in Electron Transfer. *Bull. Chem. Soc. Jpn.* **1995**, *68*, 696–712.
- (9) Yoshihara, K. Ultrafast Intermolecular Electron Transfer in Solution. *Adv. Chem. Phys.* **1999**, *107*, 371–402.
- (10) Sumi, H.; Marcus, R. A. Dynamical Effects in Electron Transfer Reactions. *J. Chem. Phys.* **1986**, *84*, 4894–4914.
- (11) Xu, Q.-H.; Scholes, G. D.; Yang, M.; Fleming, G. R. Probing Solvation and Reaction Coordinates of Ultrafast Photoinduced Electron Transfer Reactions Using Nonlinear Spectroscopies: Rhodamine 6G in Electron-Donating Solvents. *J. Phys. Chem. A* **1999**, *103*, 10348–10358.
- (12) Castner, E. W., Jr.; Kennedy, D.; Cave, R. J. Solvent as Electron Donor: Donor/Acceptor Electronic Coupling Is a Dynamical Variable. *J. Phys. Chem. A* **2000**, *104*, 2869–2885.
- (13) Scherer, P. O. J. Microscopic Models for Ultrafast Photoinduced Solvent to Dye Electron Transfer in DMA/Oxazine Solution. *J. Phys. Chem. A* **2000**, *104*, 6301–6307.
- (14) Scherer, P. O. J.; Tachiya, M. Computer Simulation Studies of Electron Transfer Parameters for Cyanoanthracene/N,N-Dimethylaniline Solutions. *J. Chem. Phys.* **2003**, *118*, 4149–4156.
- (15) Kuzmin, M. G.; Soboleva, I. V.; Dolotova, E. V. Evolution of the Reaction Mechanism during Ultrafast Photoinduced Electron Transfer. *J. Phys. Chem. A* **2008**, *112*, 5131–5137.
- (16) Morandeira, A.; Fürstenberg, A.; Gumy, J.-C.; Vauthey, E. Fluorescence Quenching in Electron-Donating Solvents. 1. Influence of the Solute-Solvent Interactions on the Dynamics. *J. Phys. Chem. A* **2003**, *107*, 5375–5383.
- (17) Morandeira, A.; Fürstenberg, A.; Vauthey, E. Fluorescence Quenching in Electron-Donating Solvents. 2. Solvent Dependence and Product Dynamics. *J. Phys. Chem. A* **2004**, *108*, 8190–8200.
- (18) Gross, L.; Mohn, F.; Moll, N.; Liljeroth, P.; Meyer, G. The Chemical Structure of a Molecule Resolved by Atomic Force Microscopy. *Science* **2009**, *235*, 1110–1114.
- (19) Schreiber, G.; Haran, G.; Zhou, H.-X. Fundamental Aspects of Protein-Protein Association Kinetics. *Chem. Rev.* **2009**, *109*, 839–860.
- (20) Boens, N.; Novikov, E.; Ameloot, M. Compartmental Modeling of Reversible Intermolecular Two-State Excited-State Processes Coupled with Rotational Diffusion or with Added Quencher. *J. Phys. Chem. A* **2005**, *109*, 7024–7023.
- (21) Baldo, M.; Grassi, A.; Raudino, A. Exact Analytical Solution of the Rotational–Translational Diffusion Equation with Mixed Boundary Conditions. An Application to Diffusion-Controlled Enzyme Reactions. *J. Chem. Phys.* **1989**, *91*, 4658–4663.

- (22) Rice, S. A. Diffusion-Limited Reactions. In *Comprehensive Chemical Kinetics*; Elsevier: Amsterdam, 1985; Vol. 25.
- (23) Burshtein, A. I. Unified Theory of Photochemical Charge Separation. *Adv. Chem. Phys.* **2000**, *114*, 419–587. Burshtein, A. I. Non-Markovian Theories Of Transfer Reactions In Luminescence and Chemiluminescence and Photo- and Electrochemistry. *Adv. Chem. Phys.* **2004**, *129*, 105–418.
- (24) Smoluchowski, M. Versuch einer Mathematischen Theorie der Koagulationskinetik Kolloider Lösungen. *Z. Phys. Chem.* **1917**, *92*, 129–168.
- (25) Rosspeintner, A.; Kattinig, D. R.; Angulo, G.; Landgraf, S.; Grampp, G.; Cuetos, A. On the Coherent Description of Diffusion-Influenced Fluorescence Quenching Experiments. *Chem.—Eur. J.* **2007**, *13*, 6474–6483.
- (26) Dorsaz, N.; De Michele, C.; Piazza, F.; De Los Rios, P.; Foffi, G. Diffusion-Limited Reactions in Crowded Environments. *Phys. Rev. Lett.* **2010**, *105*, 120601–1–4.
- (27) Zhou, H.-X.; Szabo, A. Theory and Simulation of the Time-Dependent Rate Coefficients of Diffusion-Influenced Reactions. *Biophys. J.* **1996**, *71*, 2440–2457.
- (28) Gorelik, E. V.; Lukzen, N. N.; Sagdeev, R. Z.; Murai, H. Application of Integral Encounter Theory to Account for Spin Effects in Radical Reactions: Photochemical Generation and Spin Selective Recombination of Radical Ions. *Phys. Chem. Chem. Phys.* **2003**, *5*, 5438–5443.
- (29) Kattinig, D. R.; Rosspeintner, A.; Grampp, G. Fully Reversible Interconversion between Locally Excited Fluorophore, Exciplex, and Radical Ion Pair Demonstrated by a New Magnetic Field Effect. *Angew. Chem., Int. Ed.* **2008**, *47*, 960–962.
- (30) Swallen, S. F.; Weidemaier, K.; Tavernier, H. L.; Fayer, M. D. Experimental and Theoretical Analysis of Photoinduced Electron Transfer: Including the Role of Liquid Structure. *J. Phys. Chem.* **1996**, *100*, 8106–8117.
- (31) Rosspeintner, A.; Kattinig, D. R.; Angulo, G.; Landgraf, S.; Grampp, G. The Rehm–Weller Experiment in View of Distant Electron Transfer. *Chem.—Eur. J.* **2008**, *14*, 6213–6221.
- (32) Angulo, G.; Kattinig, D. R.; Rosspeintner, A.; Grampp, G.; Vauthey, E. On the Coherent Description of Diffusion-Influenced Fluorescence Quenching Experiments II: Early Events. *Chem.—Eur. J.* **2010**, *16*, 2291–2299.
- (33) Ivanov, K. L.; Lukzen, N. N. Diffusion-Influenced Reactions of Particles with Several Active Sites. *J. Chem. Phys.* **2008**, *128*, 155105 1–5.
- (34) Solc, K.; Stockmayer, W. H. Kinetics of Diffusion-Controlled Reaction between Chemically Asymmetric Molecules. I. General Theory. *J. Chem. Phys.* **1971**, *54*, 2981–2988.
- (35) Temkin, S. I.; Jakobson, B. I. Diffusion-Controlled Reactions of Chemically Anisotropic Molecules. *J. Phys. Chem.* **1984**, *88*, 2679–2682.
- (36) Traytak, S. D.; Price, W. S. Exact Solution for Anisotropic Diffusion-Controlled Reactions with Partially Reflecting Conditions. *J. Chem. Phys.* **2007**, *127*, 184508-1–8.
- (37) Williams, R. M. Distance and Orientation Dependence of Photoinduced Electron Transfer through Twisted, Bent and Helical Bridges: a Karplus Relation for Charge Transfer Interaction. *Photochem. Photobiol. Sci.* **2010**, *9*, 1018–1026.
- (38) Adams, P. D.; Chen, Y.; Ma, K.; Zagorski, M. G.; Sönnichsen, F. D.; McLaughlin, M. L.; Barkley, M. D. Intramolecular Quenching of Tryptophan Fluorescence by the Peptide Bond in Cyclic Hexapeptides. *J. Am. Chem. Soc.* **2002**, *124*, 9278–9286.
- (39) Gladkikh, V. S.; Burshtein, A. I. Photoionization Affected by Chemical Anisotropy. *J. Chem. Phys.* **2007**, *126*, 014506 1–7.
- (40) Khokhlova, S. S.; Mikhailova, V. A.; Ivanov, A. I. The Influence of Changes in the Dipole Moment of Reagents on the Rate of Photoinduced Electron Transfer. *Russ. J. Phys. Chem. A* **2008**, *82*, 1024–1030.
- (41) Siders, P.; Cave, R. J.; Marcus, R. A. A Model for Orientation Effects in Electron-Transfer Reactions. *J. Chem. Phys.* **1984**, *81*, 5613–5624.
- (42) Domingue, R. P.; Fayer, M. D. Influence of Orientational Fluctuations on Electron Transfer in Systems of Donor-Acceptor Pairs. *J. Phys. Chem.* **1986**, *90*, 5141–5146.
- (43) Rubtsov, I. V.; Shirota, H.; Yoshihara, K. J. Ultrafast Photoinduced Solute–Solvent Electron Transfer: Configuration Dependence. *J. Phys. Chem. A* **1999**, *103*, 1801–1808.
- (44) Buu-Hoi, N. P.; Long, C. T. Hydrocarbures Polycycliques Aromatiques. II. La Formylation du Pérylène et du 3-Méthylpérylène. *Recl. Trav. Chim. Pays-Bas* **1956**, *75*, 1221–1226.
- (45) Frenkel, D.; Smit, B. Understanding Molecular Simulation: From Algorithms to Applications; Academic Press, Inc.: Orlando, FL, USA, 1996.
- (46) Cuetos, A.; Martinez-Haya, B. Columnar Phases of Discotic Spherocylinders. *J. Chem. Phys.* **2008**, *129*, 214706 1–7.
- (47) Weidemaier, K.; Tavernier, H. L.; Swallen, S. F.; Fayer, M. D. Photoinduced Electron Transfer and Geminate Recombination in Liquids. *J. Phys. Chem. A* **1997**, *101*, 1887–1902.
- (48) Koch, M.; Rosspeintner, A.; Angulo, G.; Vauthey, E. Bimolecular Photoinduced Electron Transfer in Imidazolium-Based Room-Temperature Ionic Liquids Is Not Faster than in Conventional Solvents. *J. Am. Chem. Soc.* **2012**, *134*, 3729–3736.
- (49) Newton, M. D. Electron Transfer: Theoretical Models and Computational Implementation. In *Electron Transfer in Chemistry*; Balzani, V., Ed.; Wiley-VCH: Weinheim Germany, 2001; Vol. 1.
- (50) Subotnik, J. E.; Cave, R. J.; Steele, R. P.; Shenvi, N. The Initial and Final States of Electron and Energy Transfer Processes: Diabatization as Motivated by System-Solvent Interactions. *J. Chem. Phys.* **2009**, *130*, 2341021–14.
- (51) Subotnik, J. E.; Vura-Weis, J.; Sodt, A. J.; Ratner, M. A. Predicting Accurate Electronic Excitation Transfer Rates via Marcus Theory with Boys or Edmiston–Ruedenberg Localized Diabatization. *J. Phys. Chem. A* **2010**, *114*, 8665–8675.
- (52) Vura-Weis, J.; Newton, M. D.; Wasielewski, M. R.; Subotnik, J. E. Characterizing the Locality of Diabatic States for Electronic Excitation Transfer by Decomposing the Diabatic Coupling. *J. Phys. Chem. C* **2010**, *114*, 20449–20460.
- (53) Chen, H.; Ratner, M. A.; Schatz, G. C. Time-Dependent Theory of the Rate of Photo-Induced Electron Transfer. *J. Phys. Chem. C* **2011**, *115*, 18810–18821.
- (54) Banerji, N.; Angulo, G.; Barabanov, I.; Vauthey, E. Intramolecular Charge-Transfer Dynamics in Covalently Linked Perylene–Dimethylaniline and Cyanoperylene–Dimethylaniline. *J. Phys. Chem. A* **2008**, *112*, 9665–9674.
- (55) Gladkikh, V.; Burshtein, A. I.; Rips, I. Variation of the Resonant Transfer Rate When Passing from Nonadiabatic to Adiabatic Electron Transfer. *J. Phys. Chem. A* **2005**, *109*, 4983–4988.
- (56) Kakitani, T.; Yoshimori, A.; Mataga, N. Effects of the Donor-Acceptor Distance Distribution on the Energy Gap Laws of Charge Separation and Charge Recombination Reactions in Polar Solutions. *J. Phys. Chem.* **1992**, *96*, 5385–5392.
- (57) Walker, G.; Aakesson, E.; Johnson, A.; Levinger, N.; Barbara, P. Interplay of Solvent Motion and Vibrational Excitation in Electron-Transfer Kinetics: Experiment and Theory. *J. Phys. Chem.* **1992**, *96*, 3728–3736.
- (58) Engleitner, S.; Seel, M.; Zinth, W. Nonexponentialities in the Ultrafast Electron-Transfer Dynamics in the System Oxazine 1 in N,N-Dimethylaniline. *J. Phys. Chem. A* **1999**, *103*, 3013–3019.
- (59) Seki, K.; Wojcik, M.; Tachiya, M. Diffusion-Mediated Geminate Reactions under Excluded Volume Interactions. *Phys. Rev. E* **2012**, *85*, 011131 1–13.
- (60) Nocera, D. G.; Gray, H. B. Electron Transfer Chemistry of the Luminescent Excited State of Octachlorodirhenate(III). *J. Am. Chem. Soc.* **1981**, *103*, 7349–7350.
- (61) Hou, Y.; Higashiya, S.; Fuchigami, T. Electrolytic Partial Fluorination of Organic Compounds. Part 34. Regioselective Anodic Fluorination of Benzyl Thiocyanate and Its Derivatives. *Electrochim. Acta* **2000**, *45*, 3005–3010.
- (62) Shirota, H.; Pal, H.; Tominaga, K.; Yoshihara, K. Substituent Effect and Deuterium Isotope Effect of Ultrafast Intermolecular

Electron Transfer: Coumarin in Electron-Donating Solvent. *J. Phys. Chem. A* **1998**, *102*, 3089–3102.

(63) Riddick, J. A.; Bunger, W. B.; Sakano, T. K. *Organic Solvents. Physical Properties and Methods of Purification*; John Wiley & Sons: New York, 1986.

(64) Rosspeintner, A.; Angulo, G.; Vauthey, E. Driving Force Dependence of Charge Recombination in Reactive and Nonreactive Solvents. *J. Phys. Chem. A* **2012**, *116*, 9473–9483.